Meteorite impacts on ancient oceans opened up multiple NH3 production pathways

Shimamura, Kohei
Shimojo, Fuyuki
Nakano, Aiichiro
Tanaka, Shigenori

(Citation)
Physical Chemistry Chemical Physics,19(18):11655-11667

(Issue Date)
2017-05-14

(Resource Type)
journal article

(Version)
Accepted Manuscript

Journal Name

ARTICLE TYPE

Cite this: DOI: 10.1039/xxxxxxxxxx

Meteorite Impacts on Ancient Ocean Opened Up Multiple NH_3 Production Pathways†

Kohei Shimamura,*[a] Fuyuki Shimojo,[b] Aiichiro Nakano,[c] and Shigenori Tanaka*[a]

Received Date
Accepted Date

DOI: 10.1039/xxxxxxxxxx

www.rsc.org/journalname

Recent series of shock experiments by Nakazawa *et.al.* starting in 2005 (*e.g.* [Nakazawa *et al., Earth Planet. Sci. Lett.*, 2005, **235**, 356] suggested that meteorite impacts on ancient ocean would have yielded a considerable amount of NH_3 to the early Earth from atmospheric N_2 and oceanic H_2O through reduction by meteoritic iron. To clarify the mechanisms, we imitated the impact events by performing *ab initio* molecular dynamics in the framework of density functional theory in combination with multi-scale shock technique (MSST) simulations. Our previous simulations with impact energies close to that of the experiments revealed that a picosecond-order rapid NH_3 production during shock compression [Shimamura *et al., Sci. Rep.*, 2016, **6**, 38952]. It was also shown that the reduction of N_2 took place with an associative mechanism as seen in the catalysis of nitrogenase enzyme. In this study, we performed an MSST-AIMD simulation to investigate the production by the meteorite impacts with higher energies, which are closer to the expected values on the early Earth. It was found that the amount of NH_3 produced further increased. We also found that the increased NH_3 production is due to emergence of multiple reaction mechanisms at increased impact energies. We elucidated that the reduction of N_2 was not only to the associative mechanism but also to a dissociative mechanism as seen in the Haber-Bosch process and to a mechanism through a hydrazinium ion . The emergence of such multiple production mechanisms capable of providing a large amount of NH_3 would support the suggestions from the recent experiments much more strongly than was previously believed, *i.e.*, shock-induced NH_3 production played a key role in the origin of life on Earth.

1 Introduction

NH_3 is a molecule indispensable for the birth of life on the primitive Earth. This is because NH_3 is thought to have played an important role as a relevant nitrogen source for abiotic amino acid synthesis such as Strecker reaction.[1] However, the nitrogen compound predominant on the early Earth was not NH_3 but, similar to the current Earth, the chemically inert N_2 .[2,3] Current life has acquired it by biological nitrogen fixation from N_2 by the nitrogenase enzyme.[4] In addition, human beings have established chemical nitrogen fixation by the Haber-Bosch method for the purpose of fertilizer production, and produce huge amounts of NH_3 annually.[5] In the absence of such established production methods, the question of how NH_3 was originally produced on the early Earth is an important issue related to the origin of life. Many experimental and theoretical studies[6–9] have been conducted to investigate the mechanisms of NH_3 production on the early Earth. Concerning these studies, Nakazawa *et al.*[10] suggested experimentally that meteorite impacts on the prebiotic ocean could produce a large amount of NH_3 from atmospheric N_2 and sea water by reduction of N_2 molecules by abundant metallic iron contained in the meteorites. Their experiments were conducted from the viewpoint that meteorites had rich metallic iron during the Late Heavy Bombardment (LHB) period based on previous studies. For example, Bottke *et al.*[11] suggested that the impactors during the LHB period came from the E-belt that existed around the Mars transverse zone. Most E-belt asteroids are believed to have acquired a trajectory similar to the trajectory of Hungarian asteroids containing a large amount of metallic iron. According to a rough estimate using the observed nitrogen conversion rate from the experiment by Nakazawa *et al.*,[10] the product amount during the LHB pe-

[a] *Graduate School of System Informatics, Kobe University, 1-1 Rokkodai, Nada-ku, Kobe 657-8501, Japan. Fax: +81 78 803 6621; Tel: +81 78 803 6619; E-mail: shimamura@port.kobe-u.ac.jp, tanaka2@kobe-u.ac.jp*

[b] *Department of Physics, Kumamoto University, 2-39-1 Kurokami, Chuo-ku, Kumamoto 860-8555, Japan.*

[b] *Collaboratory for Advanced Computing and Simulations, Department of Physics & Astronomy, Department of Computer Science, Department of Chemical Engineering & Materials Science, and Department of Biological Sciences, University of Southern California, Los Angeles, CA 90089-0242, USA.*

† Electronic Supplementary Information (ESI) available: A rough estimate of production amount of NH_3 based on the 6 km/s shock-wave simulation results was shown. Another desorption process of an NH_3 fragment in the dissociative mechanism was also described. See DOI: 10.1039/b000000x/

riod reaches 1.1×10^7 tons yr^{-1},[12] which corresponds to 7% of the current annual production amount by the Haber-Bosch process (1.6×10^8 tons yr^{-1}).[5] Such a source of NH_3 would have been comparable in magnitude to the proposed mineral-catalyzed reduction of crustal N_2 under oceanic hydrothermal systems,[6,7] oceanic reduction by Fe^{2+},[8] and terrestrial TiO_2 photochemical catalysis of atmospheric N_2.[9] Therefore, the hypothesis of NH_3 production induced by meteorite impacts on the ocean can be considered to be relevant as one of the production models on the early Earth.

However, this production model currently has some fundamental problems. Although a Haber-Bosch like reaction process from the similarity of their experimental conditions was assumed by Furukawa *et al.*,[13] from the similarity of their experimental conditions, the production process has not actually been clarified. It is also not well understood whether the production occurred during period of shock compression immediately after an impact or in the subsequent cooling process. Furukawa *et al.*[14–16] recently succeeded in producing at most nine types of proteinogenic amino acids and two types of nucleobases by impacting a sample containing NH_3 as a nitrogen source. Therefore, elucidation of the shock-induced NH_3 production process is quite important for understanding the production mechanism of important nitrogen precursors of fundamental biomolecules such as amino acids. It is worth noting that the meteorite impact-induced NH_3 production could be a probable model for providing NH_3 on Mars as well as on Earth, according to previous studies which suggested that atmospheric N_2[17] and spacious ocean[18] existed during the LHB period.

In order to address these issues, we performed computer simulations based on *ab initio* molecular dynamics (AIMD) method. Moreover, to reproduce atomic motions during the passing of a shock wave generated by the meteorite collision, we used Multi-Scale Shock Technique (MSST) method[19,20] in combination with the AIMD simulation (referred to as MSST-AIMD simulation).

In our previous study,[12] a simple initial atomic configuration consisting of N_2, H_2O, and metallic iron was created with reference to the sample composition of the experiment,[10] imitating the early Earth's environment during the LHB period (see Fig. 1(a)). Then, two MSST-AIMD simulations were performed, where two practical shock waves with different speeds of 4 and 5 km/s were given. While the former was prepared to reproduce the experimental conditions[10] of pressure, temperature, and impact velocity, the latter was to realize a higher energy condition. We confirmed the rapid NH_3 production in the MSST-AIMD simulation with the higher energy shock wave during shock compression. The NH_3 production occurred three times within 4 ps. On the other hand, in the simulation reproducing the experimental condition, no production was observed within the same time range. These results make one expect an increase in the amount of produced NH_3 molecules by giving higher impact velocities than that of the experiment. Besides, we found that the NH_3 molecules were produced only by an *associative mechanism* of a N_2 molecule,[21,22] *i.e.*, after the top N atom of a N_2 molecule adsorbed on the Fe slab surface as shown in Figs. 1(a) or 1(b) was hydrogenated, an NH_3 molecule was produced by dissociation of the bond between the N atoms. The detailed reaction process is described in subsection 3.2.

In this paper, to investigate the possibility of increasing the amount of produced NH_3 molecules, a MSST-AIMD simulation with a shock wave having higher speed of 6 km/s than our previous study was carried out. This is because, as described in subsection 3.1, the impact energies of the experiments[10] and our previous MSST-AIMD simulations[12] may be smaller than the actual those. A total of ten NH_3 production reactions occurred during 4 ps and five NH_3 molecules remained at 4 ps, exceeding the previous study. The reason of the increase is due to multiple reaction mechanisms to be appeared. In this simulation, NH_3 molecules were produced not only by the associative mechanism but also by *dissociative mechanism* of a N_2 molecule and reduction of a N_2 molecule through the formation of a hydrazinium ion. Since there is a possibility that these production mechanisms play significant roles, a meteorite collision with a higher velocity would further increase the amount of NH_3 molecules produced after the shock.

2 Method of Calculation

We used a system consisting of a Fe_{36} slab, 16 N_2, and 38 H_2O molecules (a total of 182 atoms; see Fig. 1(a)), which is the same one as in our previous study,[12] where the ratio of Fe atoms, N atoms, and H_2O molecules nearly coincided with that in the experimental starting material.[10] This system represents the initial reactions when a meteorite (the Fe_{36} slab) with adsorbed atmospheric N_2 collides with the sea surface while engulfing other atmospheric N_2. To investigate various reactions, we created such a model with high N_2 concentration. A rectangular supercell of dimensions 29.72 Å × 8.580 Å × 8.580 Å under a periodic boundary condition was employed. Structural optimization by Quasi-Newton method[23] was performed to prepare an initial atomic configuration. Using this atomic configuration, we performed a MSST-AIMD simulation, in which shock waves propagated in the x direction with a shock speed of 6 km/s. In our MSST-AIMD simulation, electronic states were calculated using the projector-augmented-wave (PAW) method based on density functional theory (DFT).[24,25] Projector functions were generated for the $2s$ and $2p$ states of N and O atoms, the $1s$ state for H, and the $3d$, $4s$, and $4p$ states of Fe atoms. The generalized gradient approximation[26] was used for the exchange-correlation energy with non-linear core corrections.[27] Spin polarization effects were not included here, which is a reasonable approximation as the following consideration suggests. As described in subsection 3.1, the temperature in our MSST-AIMD simulation far exceeded the Curie temperature of iron (1,043 K). Thus, the iron in our simulation would exhibit paramagnetism rather than ferromagnetism, leading to a similar result without spin polarization. In our previous AIMD simulations of similar high-temperature reactions, we compared spin-restricted and spin-unrestricted DFT calculations and indeed found that spin polarization plays a negligible role.[28] The DFT-D method was employed for the semi-empirical correction of the van der Waals interaction.[29] The momentum-space formalism[30] was utilized, where the plane-wave cutoff energies were set to be 30 and 250 Ry for the electronic pseudo-wave functions and the pseudo-charge density, respectively. The Γ point

was used for Brillouin zone sampling. The energy functional was minimized iteratively using a preconditioned conjugate-gradient method.[31,32] The MSST[19,20] was used to simulate a stable planar shock wave by correcting the equations of motion of atoms so that the volume of the simulation cell evolved over time, while imposing constraints on the Rayleigh line for the stress and the Hugoniot relation for the energy.[33] The dynamics of the system is governed by the extended Lagrangian,

$$L = \frac{1}{2}\sum_i m_i(\mathbf{h}\dot{\boldsymbol{q}}_i)^t(\mathbf{h}\dot{\boldsymbol{q}}_i) - \Phi(\{\mathbf{h}\boldsymbol{q}_i, \mathbf{h}\}) + \frac{Q}{2M}\dot{V}^2 + \frac{1}{2}MV_s^2\left(1-\frac{V}{V_0}\right)^2 - P_0(V-V_0) \quad (1)$$

where m_i is the mass of the ith atom, $\boldsymbol{q}_i$ is a column vector whose components are the ith atom's scaled coordinates in the range of [0, 1], Φ is the potential energy, Q is a parameter with unit of (mass)^2·(length)$^{-4}$, $M = \sum_i m_i$ is the total mass of the system, and V_s is the speed of the shock wave. The real coordinate and the velocity of the ith atom are given by $\mathbf{h}\boldsymbol{q}_i$ and $\mathbf{h}\dot{\boldsymbol{q}}_i$ respectively, where $\mathbf{h} = (\boldsymbol{L}_1\ \boldsymbol{L}_2\ \boldsymbol{L}_3)$ is a matrix consisting of the computational cell lattice vectors $\boldsymbol{L}_k$ (k = 1, 2, and 3). $V = \det \mathbf{h}$ is the volume of the computational cell. P_0 and $V_0 = \det \mathbf{h}_0$ are the pressure and volume of the unshocked state, respectively, where $\mathbf{h}_0$ corresponds to $\mathbf{h}$ in the unshocked state. In eq. (1), a dot denotes time derivative. Initial pressure and temperature were set to 0 GPa and 300 K, respectively. The equations of motion were integrated numerically with a time step of 10 a.u. (= 0.242 fs). Note that one specifies the shock speed (V_s) in the MSST, and we set V_s = 6 km/s in this study. The MSST-AIMD simulation was performed for the time duration of 4 ps.

To quantify the change in the bonding properties of atoms associated with production reactions of NH_3 molecules, we used a population analysis[34,35] by expanding the electronic wave functions in an atomic-orbital basis set.[36,37] Based on the formulation generalized to the PAW method,[38] we obtained the bond-overlap population (BOP or $O_{ij}(t)$) between ith and jth atoms and the gross population $Z_i(t)$ for ith atom. The Mulliken charge $Q_i(t)$ was then obtained as the difference between the number of valence electrons of an isolated neutral atom $Z_i^0(t)$ and the value of the gross population $Z_i(t)$:

$$Q_i(t) = Z_i^0(t) - Z_i(t). \quad (2)$$

We estimated the charges of the atoms from $Q_i(t)$. $O_{ij}(t)$ gives a semi-quantitative estimate of the strength of covalent bonds between atoms. Note that a bonding state exists between ith and jth atoms if O_{ij} shows a positive value. In contrast, when O_{ij} shows a negative value, an antibonding state exists. The charge spillage estimating the expansion error[36] is about 0.4%, which indicates the high accuracy of the atomic-orbital basis set.

By calculating free energies, we evaluated activation energies for the production of an NH_3 molecule by the dissociative mechanism. For this purpose, additional constant-temperature and -volume AIMD simulations were performed at T = 300 K by imposing geometrical constraints to obtain the free energy profile[39] along the NH_3 production reaction path. The Lagrange multiplier $\langle\lambda\rangle$ was introduced to constrain the interatomic distance r_{N-Fe} between one N and one Fe atoms to be reacted. By taking time average, we obtained the average Lagrange multiplier $\langle\lambda\rangle$. A constant-temperature and -volume AIMD simulation based on the Nosé-Hoover thermostat technique[40] was performed for 1 ps at each interatomic distance r_{N-Fe}. The $\langle\lambda\rangle$ becomes zero at an equilibrium interatomic distance r_0. On the other hand, the value of r_{N-Fe} is increased from this distance, and again $\langle\lambda\rangle$ becomes zero at which an NH_3 molecule is produced. The relative free energies ΔF were obtained for $r_0 > r_{N-Fe} > r_d$ by the following integral:[41]

$$\Delta F = \int_{r_0}^{r_d}\langle\lambda(r')\rangle dr'. \quad (3)$$

We calculated the free energy profiles along the corresponding reaction path using the following two models,

(a) 1 Fe_{15} cluster + 1 NH_3 fragment

(b) 1 Fe_{15} cluster + 1 NH_3 fragment + 1 N atom.

The details of the models are described in the subsection 3.4.

We used our own AIMD code,[42] which has been implemented on parallel computers using the message passing interface library for interprocessor communications.

3 Results and Discussions

3.1 Time Evolution of Physical Quantities

Before discussing NH_3 productions, we first discuss the time evolution of four physical quantities, *i.e.*, the volume ratio (V/V_0 with V_0 being the initial volume), pressure (P), particle velocity (U_p), and temperature (T) as shown in Figs. 2(a)-(d). In particular, since the particle velocity is comparable to actual impact velocity of meteorites, it is an essential quantity to characterize the reality of simulation. For all the four quantities, there were rapid changes at around 0.2 ps. The respective values of V/V_0, P, and U_p converged to 0.50, 43.0 GPa, and 3.00 km/s at 4 ps. In contrast, the temperature rapidly increased at around 0.2 ps, and subsequently it gradually increased from around 2,450 to 3,180 K. This indicates that some exothermic reactions occur. For comparison, the values of the volume ratio, pressure, particle velocity, and temperature at 4 ps in the 5 km/s shock-wave simulation[12] were 0.58, 27.6 GPa, 2.30 km/s, and 2,100 K, respectively. Due to the higher compression ratio ($V/V_0 = 0.50 < 0.58$), P, U_p, and T of the present simulation were greater than those of the previous one. Such higher pressure and temperature in the 6 km/s shock-wave simulation increased the reactivity and accelerated the NH_3 production reactions as described in the following subsections.

Meanwhile, the particle velocity of our simulation would be in a realistic impact velocity range. It is much slower than a typical meteorite's impact velocity (above 10 km/s),[43] but this typical velocity does not account for the effects of aerobraking by the Earth's atmosphere[44] and of deceleration of breakup while passing through the atmosphere.[45] Even if the initial velocity before entering the atmosphere is 10 km/s or more, considering these effects, the impact velocity on the planetary surface could be about 1 km/s.[45] This would be comparable to the present simulation.

However, it should be also mentioned that these deceleration effects of meteorites strongly depend on the density of the atmosphere. The density of the early atmosphere is still uncertain, thus the deceleration effects would be weakened if the density was lower than what was assumed in ref. 44 (where the current atmospheric density was used). Taking into account such possibilities, we will continue to implement MSST-AIMD simulations with shock waves having further greater speeds in the future.

3.2 Time Evolution of Number of Produced NH_3 Molecules

Here, the number of produced NH_3 molecules in the 6 km/s shock-wave simulation and the outline of the production processes are described. Figure 2(e) shows the time evolution of the cumulative number of produced NH_3 molecules or NH_4^+ ions (solid line) and of remaining number of the produced NH_3 molecules or NH_4^+ ions (dashed line) in the 6 km/s shock-wave simulation. In total, 10 NH_3 molecules were produced (noted with [a]-[i]). Five of these produced NH_3 molecules have broken, but other five remained at 4 ps, which is more than that in the 5 km/s shock-wave simulation.[12] The reason why the five NH_3 molecules were broken is described in subsection 3.4. The increase in the production amount is due to the production mechanism, as addressed below.

We reported that all the NH_3 production that occurred in the 5 km/s shock-wave simulation was due to an *associative mechanism* of N_2 on the Fe slab surface. A N_2 molecule, of which one N atom (bottom N atom) is bonded on the Fe slab surface as shown in Figs. 1(b) and 1(c), becomes an ammoniacal nitrogen (NH_3-N) by hydrogenating the other N atom (top N atom), and finally an NH_3 molecule is produced by breaking the bond between the two N atoms. This is analogous to the mechanism in the nitrogenase enzyme.[21,22] We found that the formation of tetra-coordinate with the Fe atoms for the bottom N atom triggered cleavage of the bond of N-N and an NH_3 production. Since the temperature exceeded the melting point of metallic iron (1,810 K) and thus the mobility of Fe atoms is high, so that the number of bonds between Fe atoms and the bottom N atom can easily be increased. This is the reason why the NH_3 productions could occur within such a short period of 4 ps in the 5 km/s shock-wave simulations. Note that no production occurred in the 4 km/s shock-wave simulation, where the temperature did not exceed the melting point. However, according to previous studies,[21,22] the strict associative mechanism proceeds as follows:

$$* + N_2 \rightarrow *N_2 \tag{4}$$

$$*N_2 + 6H \rightarrow *NNH + 5H \tag{5}$$

$$*NNH + 5H \rightarrow *NNH_2 + 4H \tag{6}$$

$$*NNH_2 + 4H \rightarrow *N + NH_3 + 3H \tag{7}$$

$$*N + 3H \rightarrow *NH + 2H \tag{8}$$

$$*NH + 2H \rightarrow *NH_2 + 1H \tag{9}$$

$$*NH_2 + 1H \rightarrow *NH_3 \tag{10}$$

$$*NH_3 \rightarrow NH_3 + * \tag{11}$$

or,

$$*NNH + 5H \rightarrow *NHNH + 4H \tag{6a}$$

$$*NHNH + 4H \rightarrow *NHNH_2 + 3H \tag{7a}$$

$$*NHNH_2 + 3H \rightarrow *NH_2NH_2 + 2H \tag{8a}$$

$$*NH_2NH_2 + 2H \rightarrow *NH_2 + NH_3 + 1H, \tag{9a}$$

where $*$ denotes an adsorption site on the Fe slab surface, and the reaction eq. (9a) continues to that of eq. (10). In our 5 km/s shock-wave simulation, the desorption reaction eq. (11) did not occur. Therefore, we called it the associative mechanism for NH_3 production reaction from the top N atom (*i.e.* eqs. (7) and (9a)). In the present 6 km/s shock-wave simulation, two NH_3 molecules were produced at [c] and [d] in Fig. 2(e) by the associative mechanism of N_2 on the Fe slab surface, which is because the temperature (3,180 K at 4 ps) was much higher than the melting point of metallic iron.

On the other hand, in the 6 km/s shock-wave simulation the remaining eight NH_3 molecules were produced by different two mechanisms. Six NH_3 molecules were produced at [a] and [e]-[i] in Fig. 2(e) by a *dissociative mechanism* of N_2 on the Fe slab surface, where an NH_3 molecule was produced by desorption from the surface of the Fe slab after hydrogenation occurred in a single N atom dissociated from a N_2 molecule on the surface:[21,22]

$$2* + N_2 \rightarrow 2*N \tag{12}$$

$$2*N + 6N \rightarrow *N + *NNH + 5N \tag{13}$$

$$*N + *NNH + 5N \rightarrow 2*NH + 4N \tag{14}$$

$$2*NH + 4N \rightarrow *NH + *NH_2 + 3N \tag{15}$$

$$*NH + *NH_2 + 3N \rightarrow 2*NH_2 + 2N \tag{16}$$

$$2*NH_2 + 2N \rightarrow *NH_2 + *NH_3 + 1N \tag{17}$$

$$*NH_2 + *NH_3 + 1N \rightarrow 2*NH_3 \tag{18}$$

$$2*NH_3 \rightarrow *NH_3 + NH_3 + * \tag{19}$$

$$*NH_3 + NH_3 + * \rightarrow 2NH_3 + 2*. \tag{20}$$

Production in the Haber-Bosch process proceeds along this dissociative mechanism.[21,22] It should be noted that the reactions eqs. (8)-(11) in the strict associative mechanism cannot be distinguished from the case of one N atom of the dissociative mechanism except for the reaction eq. (12). Actually, in the 6 km/s shock-wave simulation, NH_3 production by the strict associative mechanism occurred once, where two NH_3 molecules were produced from top and bottom N atoms at [c] and [f] in Fig. 2(e). However, since the production process at [f] was equivalent to that by the dissociation mechanism except the reaction eq. (12), it was counted as a production by the dissociation mechanism. The question is why the desorption reaction eq. (11) (or (19) and (20)) occurred in the 6 km/s shock-wave simulation, which is involved with the rapid NH_3 production. The reason is discussed in subsection 3.4.

The remaining two NH_3 molecules were produced from those N_2 molecules which were not adsorbed on the Fe slab surface.

By receiving H atoms, a hydrazinium ion ($N_2H_6^{2+}$) was firstly formed from a N_2 molecules away from the Fe slab, and then two NH_3 molecules were produced at [b] in Fig. 2(b). $N_2H_6^{2+}$ ions have been regarded as precursors to produce NH_3 from N_2 using an electrocatalyst in previous studies.[22,46–48] While we have confirmed the production of ion in the 5 km/s shock-wave simulation in our study,[12] two productions were observed at 0.535 ps and 1.500 ps in the 6 km/s shock-wave simulation. Although the first formed ion was deconstructed at 1.181 ps by bonding with Fe atoms, the second ion became two NH_3 molecules at 1.663 ps. The detail reaction processes are discussed in subsection 3.6.

Due to the addition of two production mechanisms to the associative mechanism, increase in the production amount could be expected if an experiment with a higher impact velocity is executed. Especially, since the production by the dissociative mechanism was the most frequent, this mechanism would be responsible for those in real meteorite impacts, as inferred by Furukawa *et al.*[13] Although our calculation model has quite high N_2 concentration, it is worth mentioning that the annual production amount of NH_3 during shock compression is estimated to be about 7.2×10^7 tons (see Supplementary Information), which is larger than the estimated annual production amounts from our 5 km/s shock-wave simulation (4.3×10^7 tons) and from the shock experiment by Nakazawa *et al.* (1.1×10^7 tons). This result also implies that shocks with greater impact velocities would increase the yield of NH_3. In fact, in order to estimate the exact amount of produced NH_3, it is necessary to reproduce the quenching process after the shock compression.[49,50] We plan to perform additional AIMD simulations of about 100 ps as a future work. However, the rapid production of NH_3 during shock compression is important because it would be an ingredient for biomolecules such as amino acids. Previous shock studies[15,49] that succeeded in the production of amino acids assumed that a large amount of NH_3 molecules existed before the meteorite collisions. In addition, Goldman *et al.*[49] have confirmed the formation of glycine, which is one of amino acids, during the quenching process after the shock compression using AIMD simulations. If the production of biomolecules such as amino acids occurs in the quenching process, the NH_3 molecules observed in our simulations potentially become the ready-to-use ingredient, and makes one expect the production of biomolecules from not pre-existing NH_3 but atmospheric N_2.

The following subsection 3.3 describes dehydrogenation mechanism of H_2O molecules, which is a key to NH_3 production as a source of H atoms. In subsection 3.4, the production processes by the dissociative mechanism is discussed. Subsections 3.5 and 3.6 describe the formation reaction of a $N_2H_6^{2+}$ ion and the subsequent NH_3 production process, respectively. In subsections 3.4, 3.5, and 3.6, we also elucidate the reason why no production based on these mechanisms occurred in the 5 km/s shock-wave simulation.

3.3 Dehydrogenation Mechanisms of H_2O molecules

Figures 2(f) and 2(g) show the time evolution of the numbers of bonds between H-O, O-Fe, H-N and H-Fe atoms in the 6 km/s shock-wave simulation. To calculate the numbers of those bonds, a bond was defined between two atoms that were within the cutoff length continuously for a prescribed lifetime. The lifetime was chosen to be 2.42 fs, and the cutoff lengths for H-O, O-Fe, H-N, and H-Fe bonds were 1.25, 1.50, 2.00, and 2.50 Å, respectively. The cutoff lengths were determined from the first minima of partial radial distribution functions obtained from the 5 km/s shock-wave simulation.[12] The lifetime and the cutoff length for H-N were also used to calculate the number of produced NH_3 molecules shown in Fig. 2(e).

The number of bonds of H-O and O-Fe in the 6 km/s shock-wave simulation reached 37 and 52 at 4 ps, respectively, indicating that H_2O molecules were dehydrogenated and the dehydrogenated O atoms oxidized the Fe slabs. The numbers of dissociated H atoms within 4 ps were 39 (= 76 - 37) and 33 for the 6 and 5 km/s simulations, respectively. A large fraction of the dissociated H atoms formed a bond with the N atom (see H-N in Fig. 2(g)), the numbers of which were 31 and 24 at 4 ps for the 6 and 5 km/s simulation, respectively. The rest existed as single atoms on the surface of Fe slab or its inside (see H-Fe in Fig. 2(g)). The corresponding numbers were 8 (= 39 - 31) and 9 for the 6 and 5 km/s simulations, respectively. (This number 8 is not in agreement with that of H-Fe at 4 ps because the single H atoms formed bonds with multiple Fe atoms). As described in next subsection 3.4, the increase in the number of dissociated H atoms from the 5 to 6 km/s simulations provided more hydrogenated N atoms on the Fe slab that played a catalytic role as well as precursors of NH_3 molecules.

As with the 5 km/s shock-wave simulation described in our previous research,[12] there were two dehydrogenation mechanisms of H_2O molecules. The first was accompanied by the densification of H_2O molecules due to sudden shock compression.[51] For example, assuming that there are two water molecules, the intermolecular H-O bond distance between H_2O molecules becomes close to the intra-molecular ones, leading to the formation of a metastable H_3O_2 cluster sharing one H atom. Then, an extra H atom is released. In the previous study,[12] we reported that the released H atoms induced proton transfers to N atoms on the Fe slab surface by Grotthuss mechanism.[52] The other mechanism was dehydrogenation of H_2O molecules adsorbed on the Fe slab surface. The O atom of adsorbed H_2O molecule released the H atoms to form bonds with Fe atoms according to the electronegativity. The released H atoms bonded to N atoms on the Fe slab surface or existed as single atoms on the surface. Furthermore, when the H atoms were released to other H_2O molecules away from the Fe slab surface, proton transfers were induced, and finally distant N atoms on the Fe slab surface often obtained them. When H atoms are supplied to N atoms on the Fe slab surface by these dehydrogenation mechanisms, coordinate bonds using a N atom's lone pairs are temporarily created, and then covalent N-H bonds are formed by receiving electrons from Fe atoms. It should be noted that transfer of H atoms between N atoms on the Fe slab surface was observed from 0.5 ps after the shock, as shown in Fig. S1 of Supplementary Information.

3.4 Dissociative Production Mechanism of an NH_3 Molecule

As described in subsection 3.2, in the dissociative mechanism, hydrogenation occurs after a N_2 molecule adsorbed on the Fe slab surface is dissociated to become a two single N atoms, and then the hydrogenated N atom is desorbed as an NH_3 molecule.[21,22] In our shock-wave simulations, such single N atoms are formed from N_2 molecules taking an adsorption configuration on the Fe slab surface as shown in Fig. 1(c). The formation of N12 shown in Fig. S1 of supplementary information is an example for the single N atoms. Since the Fe slab surface was heterogeneous, electrons were easily supplied and dissociation of N-N bonds was promoted. In addition, as described in subsection 3.3, many dissociated H atoms from H_2O molecules immediately bonded to them. Even in our 5 km/s shock-wave simulation,[12] such hydrogenated N atoms (called NH_x fragments (x = 1, 2, and 3)), precursors of NH_3 molecules, were formed on the Fe slab surface. Figure 3 shows time evolution of the number of NH_x fragments on the Fe slab surface for the 5 and 6 km/s shock-wave simulations. These fragments were rapidly formed even in the 5 km/s shock-wave simulation, and the first NH_3 fragment appeared at 0.5 ps after the shock. However, since survival time of the NH_3 fragments was quite short (< 20 fs), the fragments could not desorb from the Fe slab surface as NH_3 molecules and the production by the dissociative mechanism was not observed in the 5 km/s shock-wave simulation. On the other hand, in the 6 km/s shock-wave simulation, survival time of the NH_3 fragments was much longer. This is because the increase in the number of dissociated H atoms led to more formation of NH_1 fragments. Following this increase in the NH_1 fragments, the NH_2 and NH_3 fragments also became more abundant. Maintaining the NH_3 fragments for such a long time would be one of the important factors for rapid production of NH_3. In fact, NH_3 molecules were produced by desorption of the NH_3 fragments from the Fe slab surface at [a] and [e]-[i] in Fig. 2(e).

Furthermore, the presence of other N atoms on the Fe slab surface is the other key factor for the rapid production. It worked to weaken the bonds between the NH_3 fragments and Fe atoms and promoted the production of NH_3 (in other words, it helped desorption of NH_3 fragments). The reason could be explained using an example of the desorption reaction processes. Figure 4 shows the desorption process of an NH_3 fragment in the dissociative mechanism occurring at [e] of Fig. 2(e). Time evolution of the atomic configuration is shown in Fig. 4(a), where an NH_3 fragment consisting of N1, H2, H3, and N1 was desorbed from Fe1 at 2.568 ps. For simplicity, omitting the reaction processes that resulted in the NH_3 fragment (*e.g.,* the dissociation reaction of the N_2 molecule and the hydrogenation processes,) we start from the situation that the NH_3 fragment was formed. In addition, a NH_1 fragment consisting of N2 and H4 was present near the NH_3 fragment. As described below, this N2 played the most important catalytic role. Although the H_2O molecule containing O1 seen in Fig. 4(a) was not directly involved in the desorption, it is necessary to explain the large change of bond strengths between the H and N atoms. We address this issue at the end of this subsection. Figures 4(b) and 4(c) show the time evolution of the bond-overlap populations $O_{ij}(t)$ and the Mulliken charges $Q_i(t)$ for specified atoms using the Mulliken bond-overlap population analysis (see section 2).

An NH_3 fragment was formed by supplying H3 from surrounding H_3O^+ to N1 at 2.306 ps. Since the sum of Mulliken charges $Q_i(t)$ of N1, H1, H2, and H3 was almost zero, the production of an NH_3 molecule was likely to occur soon. However, it did not occur immediately, and the corresponding NH_3 molecule was produced at 2.568 ps after 0.3 ps. The breakage of the bonds between N and Fe atoms was needed for the production, but $O_{\mathrm{N1-Fe1}}(t)$ or $O_{\mathrm{N1-Fe2}}(t)$ had a positive value ($\sim$0.2) until 2.568 ps. NH_3 fragments cannot easily escape from the influential range of the Fe atoms even at high temperature in this way. At 2.338 ps, the bond between N1 and Fe1 was broken ($O_{\mathrm{N1-Fe1}}(t)$) reached zero). This is due to that N2 formed a strong bond with Fe1 ($O_{\mathrm{N2-Fe1}}(t)$ rapidly increased) with dissociated H4. That is, electrons from Fe1, which formed bonds with N1, were subsequently involved in the formation of bond with N2. N1 strengthened the bond with Fe2 ($O_{\mathrm{N128-Fe177}}(t)$ reached $\sim$0.3), but the bond was broken at around 2.384 ps because N2 also began to strengthen the bond with Fe2. Although N1 formed a bond with Fe1 again at around 2.372 ps (see $O_{\mathrm{N1-Fe1}}(t)$), the bond was unstable ($O_{\mathrm{N1-Fe1}}(t)$ showed zero at many times during the remaining process). In addition, since the bond of N2-Fe1 gently increased, the bond of N1-Fe1 gradually weakened the bond with Fe1. Finally, at 2.568 ps, N1 broke the bond with Fe1 and then the bond strength of N1-Fe1 reached almost zero (see $O_{\mathrm{N1-Fe1}}(t)$), *i.e.*, an NH_3 molecule was produced. In this way, NH_3 fragments can become NH_3 molecules (or can be desorbed) with the support of the N atoms such as N2. Similar catalytic reactions have been observed in previous studies using the AIMD simulations,[53,54] where H_2 production processes on Ni cluster was discussed. It was clarified that C atoms existing on the Ni cluster surface catalytically supported the desorption of H_2 molecules from the Ni cluster. In the present study, the N atoms bidentate-coordinated to Fe atoms (called N_{2Fe} atoms) such as N2 were seen in all of the desorption processes in the dissociative mechanism in the 6 km/s shock-wave simulation. For example, N12 in another desorption process occurring at 0.908 ps (see Fig. S1 in Supplement Information) played a role similar to N2. Time evolutions of the numbers of N_{2Fe} atoms in the 5 and 6 km/s shock-wave simulations are shown in Fig. 5. Compared with N_{2Fe} atoms in the 5 km/s simulation, those of the 6 km/s simulation appeared at a much higher frequency, resulting in the six NH_3 production reactions in the 6 km/s shock-wave simulation. Such N_{2Fe} atoms can be formed from the single N atoms dissociated from N_2 molecules on the Fe slab surface, as another desorption reaction shown in supplemental information. However, in many cases, the NH_1 fragments become N_{2Fe} atoms by releasing their H atoms as shown in Fig. 4(a). This reflects the fact that many NH_1 fragments were formed in the 6 km/s shock-wave simulation (see Fig. 2(e)).

We also estimated the activation free energies when an NH_3 fragment was desorbed from the surface of Fe slab as an NH_3 molecule, with and without such N_{2Fe} atoms. The calculation details were described in section 2. In order to obtain a qualitative conclusion, the free energies were calculated at 300 K, not at high

temperature of 3,180 K in the 6 km/s shock-wave simulation. The systems shown in Figs. 6(a) and 6(b) consist of a Fe_{15} cluster and a NH_3 fragment with and without a N_{2Fe} atom, respectively. We used the Fe_{15} cluster because the N_{2Fe} atom could exist during the simulations without changing the coordination number for Fe atoms even at 300K. The calculated free energy profiles are shown in Fig. 6(c). The estimated values of activation energies at 300 K were 0.65 and 0.45 eV for the cases with and without a N_{2Fe} atom, respectively. In other words, the energy barrier for NH_3 production was reduced by as much as 0.2 eV in the presence of N_{2Fe}. Also, the interaction distance between the NH_3 fragment and Fe_{15} cluster (*i.e.* r_{N-Fe}) is noteworthy. In the absence of the N_{2Fe} atom, an NH_3 molecule could be produced unless the NH_3 fragment was 4 Å away from the cluster, whereas the distance decreased to 3 Å with the atom. It is therefore concluded that the presence of N_{2Fe} atom makes two contributions: a significant decrease in activation energy and a shrinkage in the influential range of Fe atoms. In the 6 km/s shock-wave simulation, five out of ten produced NH_3 molecules were broken by recombining with Fe atoms within 4 ps (see Fig. 2(e)). The simulation cell imposed with the periodic boundary condition caused the produced NH_3 molecules to return to near the Fe slab surface. The reason why the decomposition reaction occurred is that, when the NH_3 molecule returned, there was no factor to screen the influential range of Fe atoms (such as N_{2Fe}) atoms on the Fe slab surface. In actual meteorite collisions, metallic irons likely broke up in the atmosphere or at impacts on ocean, and thus each iron cluster was surrounded by many metallic irons. Under such conditions, it is important to account for similar decompositions on nearby Fe surfaces.

At 2.618 ps, the NH_3 molecule produced at 2.568 ps immediately received one H atom from an adsorbed H_2O molecule (see $O_{H5-N1}(t)$), and then became an $NH_4{}^+$ ion. All the produced NH_3 preferred to exist as $NH_4{}^+$ under the condition of the present simulation.

Meanwhile, the bond strengths of H1-N1 and H3-N1 temporarily weakened at 2.338 and 2.355 ps, respectively. This is because N1 interchanged H atoms (H1 and H3) with a surrounding H_2O molecule, which is understandable from the fact that $O_{H1-O1}(t)$ and $O_{H3-O1}(t)$ temporarily had positive values during this period. In addition, we note that the formation of the bond between H1 and H6 at around 2.396 ps indicates temporary production of a H_2 molecule. This reflects that H1 had sufficient electrons, and the Mulliken charge of H1 momentarily reached zero.

Here, we described the detailed production process by the dissociative mechanism that occurred in our simulation, but since the N_2 molecules in our calculation model were of high concentration, the actual reaction rate is reduced somewhat due to the decrease in the number of contacts between N_2 molecules and iron. Nevertheless, once their contact occurs, an NH_3 molecules would be rapidly produced. As mentioned above, in addition to one N atom contained in an NH_3 molecule, another N atom was required to work catalytically for the rapid production. Even though there is only one N_2 molecule, a production reaction based on the dissociative mechanism would occur if the two N atoms constituting the molecule play their respective roles. In this simulation, such a reaction actually occurred once ([g] in Fig. 2(e)). In addition, the rapid production by the associative mechanism would also occur if N_2 molecules contact iron. This is because the production process does not depend on other N_2 molecules, as explained using the equations in subsection 3.2 or in our previous study.[12]

3.5 Formation Mechanism of a $N_2H_6{}^{2+}$ ion from a N_2 Molecule

In this subsection, the formation process of a $N_2H_6{}^{2+}$ ion from a N_2 molecule observed in the 6 km/s shock-wave simulation is discussed in detail, and subsequent NH_3 molecule production process by further reduction of the $N_2H_6{}^{2+}$ ion is discussed in next subsection 3.6. A $N_2H_6{}^{2+}$ ion was also confirmed to be formed even in the 5 km/s shock-wave simulation,[12] where single H atoms with abundant electrons present on the Fe slab surface were transferred into a N_2 molecule away from the Fe slab surface via several H_2O molecules with electrons based on the Grotthuss mechanism. Of the two formations occurring at 0.535 and 1.500 ps of the 6 km/s simulation, the first reaction process closely resembled that of the 5 km/s simulation, but the formed $N_2H_6{}^{2+}$ ion was broken at 1.181 ps because of bonding to Fe atoms. On the other hand, the second formation process at 1.500 ps was somewhat different from the first one. The key point for the second process is that hydrogenated N_2 molecules upright on the Fe slab surface (including NH_x fragments) mainly transferred their H atoms to a N_2 molecule directly or via some H_2O molecules. Therefore, the N_2 molecule close to these hydrogenated N_2 molecules on the Fe slab surface would potentially become a $N_2H_6{}^{2+}$ ion. Also, these hydrogenated N_2 molecules play an important role in the subsequent NH_3 production process. The formation reaction of $N_2H_6{}^{2+}$ ion and the subsequent production reaction of NH_3 were seen only once in the 6 km/s shock-wave simulation; thus there was a possibility that the reactions happened by chance. Considering that our calculation model has a high nitrogen concentration, this reaction would be more difficult to occur. However, since it can be one of the mechanisms to increase the production amount of NH_3, we describe the reaction processes in detail as follows.

The formation process of $N_2H_6{}^{2+}$ ion is shown in Fig. 7. Figure 7(a) shows time evolution of the atomic configuration, where a $N_2H_6{}^{2+}$ ion was formed at 1.500 ps by bonding five H atoms of H7, H9, H12, H14, and H15 to a N_2 molecule composed of N3 and N4. Figures 7(b) and 7(c) show the time evolution of $O_{ij}(t)$ and $Q_i(t)$ for specified atoms.

Since the sum of the Mulliken charges of N3 and N4 was nearly zero at 1.300 ps, the value 1.5 of $O_{N3-N4}(t)$ indicates the strength of the triple bond of a N_2 molecule. However, N3 started interacting with two H atoms of H7 and H8 near 1.343 ps, so that the bond strength between N3 and N4 decreased (see $O_{N3-N4}(t)$) and the Mulliken charge of N3 (see $Q_{N3}(t)$) became more negative. This is because electrons were supplied through the bonds with H7 and H8, although the bonds with two H atoms were broken at around 1.355 ps by releasing H7 and H8 to N5 and to a surrounding H_3O^+, respectively. At 1.362 ps, N3 began to interact with H7

contained in the surrounding H_3O^+ again. On the other hand, N3 also began to interact with H9 of a H_2O molecule including O3, but O3 formed a bond with H10 of H_3O^+. In other words, it could be regarded that H10 was shared by O2 and O3. Subsequently, at 1.375 ps, O3 caused proton transfers getting H10 from O2 instead of giving H9 to N3. Meanwhile, by proton transfers, O4 took away H10 from N6 and then supplied H12 to N4. At 1.379 ps, $O_{N3-N4}(t)$ showed the strength of double bond ($\sim$1.0), while the sum of Mulliken charges $Q_i(t)$ of N3, N4, H9, and H12 became almost zero. This indicates that a diazene molecule (N_2H_2) was produced. At 1.394 ps, H7 was supplied to N3 by a proton transfer, and then N4 formed a weak bond with H13 contained in a surrounding H_3O^+. These formation bonds gave rise to further weakening of the bond between N3-N4, decreasing the strength of single bonds (O_{N3-N4} reached $\sim$0.5). N4 released H13 and obtained H14 from N7 at 1.418 ps, where the sum of Mulliken charges $Q_i(t)$ of N3, N4, H7, H9, H12, and H14 became zero, *i.e.*, a hydrazine molecule (N_2H_4) was produced. After N3 formed a bond with H15 from N8 at 1.476 ps, N4 obtained H16 from a surrounding H_3O^+ at around 1.500 ps. Thus, a $N_2H_6{}^{2+}$ ion was formed. Of the six bonded H atom, five (H7, H9, H12, H14, and H15) were supplied from (both directly and indirectly via H_2O molecules) the hydrogenated N_2 molecules upright on the Fe slab surface. It is considered that the hydrogenated N_2 molecules are useful as a source of H atoms and can be somewhat away from the influential range of Fe slab. We describe in the next subsection 3.6 that these hydrogenated N_2 molecules also play an important role in the production of NH_3.

However, the sum of Mulliken charges was not equal to +2 (only +0.8) at this time, which is due to that the bond strengths of N3-H15 and N4-H16 are only half in those for other H-N bonds at 1.500 ps. That is, the $N_2H_6{}^{2+}$ ion was in a situation close to a $N_2H_5{}^+$. As described in the next subsection, therefore the $N_2H_6{}^{2+}$ ion did not immediately become two NH_3 molecules.

3.6 Production Mechanism of Two NH_3 Molecules through Reduction of a $N_2H_6{}^{2+}$ ion

In this subsection, we discuss the reaction process of NH_3 produced by reduction of the $N_2H_6{}^{2+}$ described in previous subsection 3.5. Figure 8(a) shows time evolution of the atomic configuration, where two NH_3 molecules were formed at 1.663 ps. Figures 8(b) and 8(c) show the time evolution of $O_{ij}(t)$ and $Q_i(t)$ for specified atoms.

Although the $N_2H_6{}^{2+}$ ion was formed at 1.500 ps, H12 was dissociated from N4 by proton transfers involving O5 and N9 at 1.537 ps. Furthermore, at 1.578 ps, H14 and H15 were deprived by N10 and N8 at 1.578 and 1.588 ps, respectively. In this way, the hydrogenated N_2 molecules upright on the Fe slab surface often deprives the H atoms. At 1.600 ps, the $N_2H_6{}^{2+}$ ion resulted in the state of N_2H_3, where N3 and N4 competed with each other for bonding with more H atoms and filling the hole of the deprived H atoms. It can be understood that not only $O_{H9-N3}(t)$ but also $O_{H9-N4}(t)$ had a positive value. At this time, the bond between N3 and N4 was temporarily broken, indicating that electrons between N3 and N4 were used to form bonds with H9 and the bonding state of N3-N4 became unstable. From 1.609 ps, H atoms began to be supplied to N3 and N4 again, and N4 obtained H17 from N10. At 1.624 ps, proton transfers occurred between surrounding one H_2O molecule and H_3O^+, and then H18 bonded to N3 instead of dissociating H7. At this time, the bond strength of N3-N4 increased to $\sim$0.5 again. At around 1.638 ps, N3 and N4 obtained H8 and H13 again from N5 and the surrounding H_3O^+, respectively (see the snapshots at 1.343 and 1.418 ps in Fig. 7(a)). Although a $N_2H_6{}^{2+}$ ion was formed again, the bond strength between N3 and N4 could not be restored and reached zero at around 1.663 ps, leading to the production of two NH_3 molecules. The sums of Mulliken charges for the respective two NH_3 molecules also became zero.

As stated above, competing H atoms between N3 and N4 would give rise to an instability of the N3-N4 bond, thus resulting in the NH_3 production. Then, it is considered that active exchange of H atoms with the hydrogenated N_2 molecules on the Fe slab surface is an important factor. Figure 9 shows time evolution of the numbers of N_2 molecules bonded by one or more H atoms upright on the Fe slab surface in the 5 and 6 km/s shock-wave simulations. It can be seen that there are more hydrogenated N_2 molecules formed between 1.343 and 1.663 ps in the 6 km/s shock-wave simulation, where the formation of the $N_2H_6{}^{2+}$ ion and the production of two NH_3 molecules occurred. It is therefore concluded that NH_3 could be produced when many hydrogenated N_2 upright on Fe surfaces exist. A plausible reason why it did not occur in the 5 km/s shock-wave simulation is because there were not enough hydrogenated N_2 molecules on the Fe slab surface.

In this way, NH_3 production from hydrazinium ions might largely depend on the number of surrounding N_2 molecules. Only one production was observed even in our calculation model with high N_2 concentration, which indicates that this reaction is extremely rare in reality. N_2 molecules that were placed in special situations, such as those near meteorites with a large amount of atmospheric N_2 molecules adsorbed on the surface, would be an object of the NH_3 production mechanism. Meanwhile, hydrazinium ions themselves could be formed by another mechanism different from the one in subsection 3.5, *i.e.*, through single H atoms existing on the Fe slab surface found in our previous study.[12] We have not yet observed a case where hydrazinium ions formed by this mechanism produce NH_3 molecules. The corresponding ion was broken at 1.181 ps in the 6 km/s simulation, whereas it remained intact even at 4 ps in the 5 km/s simulation. Therefore, we will elucidate whether the ion is transformed to NH_3 molecules, for example, by performing a long-term calculation considering the cooling process from the state at 4 ps of the 5 km/s shock-wave simulation.

4 Conclusions

By means of an AIMD combined with MSST method, we simulated a shock wave generated by a meteorite impact on ancient ocean with a larger speed 6 km/s than the previous ones[12] (5 and 4 km/s) for a system consisting of metallic iron, N_2, and H_2O, imitating the prebiotic Earth during the LHB period. The results suggested that meteorite impacts with the larger speed could further increase the amount of NH_3 molecules produced immediately af-

ter the shock (*i.e.* shock compression).

This is because the NH_3 production occurred not only by the associative mechanism observed in the 5 km/s shock-wave simulation,[12] but also by following two different production mechanisms. The one is the dissociative mechanism, where a single N atom is formed from the decomposition of a N_2 molecule on the Fe slab surface, and then the single N atom bonded by three H atoms (NH_3 fragment) was desorbed from the surface. Although the formation of the NH_3 fragments has already been confirmed even in the 5 km/s shock-wave simulation, they have never been desorbed from the Fe slab surface due to their short life time (< 20 fs). One of the reasons that the desorption reaction rapidly occurred in the 6 km/s simulation is because the number of decomposed H atoms from H_2O was larger than that in the 5 km/s shock-wave simulation, leading to increases in the number of hydrogenated N atoms on the Fe slab surface (*i.e.* NH_1 fragment, NH_2 fragments, and NH_3 fragments) and in survival time of the NH_3 fragments. The other reason is a catalytic function by other N atoms on the Fe slab surface. We found that the N atoms bidentate-coordinated to Fe atoms deprive the electrons used to form the bonds between Fe atoms and NH_3 fragment, thereby accelerating the desorption as an NH_3 molecule.

Another production mechanism is the reduction of a N_2 molecule through the formation of a $N_2H_6{}^{2+}$ ion, where a N_2 molecule was reduced by H atoms and then two NH_3 molecules were produced. The $N_2H_6{}^{2+}$ ion itself was also formed in the 5 km/s shock-wave simulation, but none of the bond of N-N was broken. In the 6 km/s shock-wave simulation, on the other hand, this reduction reaction would be enhanced by high exchange of H atoms between a $N_2H_6{}^{2+}$ ion and hydrogenated N_2 molecules upright on the Fe slab surface. Such intense exchange rate of H atoms destabilized the bond of N-N, resulting in the rapid NH_3 production. It is considered that the number of the hydrogenated N_2 molecules in the 5 km/s shock-wave simulation was insufficient to lead to the intense exchange of H atoms.

Meteorite impacts leading to such multiple production mechanisms may have resulted in a tremendous amount of NH_3 on the early Earth, which strongly supports the experimental suggestions.[10,13–15]

Acknowledgements

We would like to express our deepest and sincere gratitude to Professor Hiromoto Nakazawa, National Institute for Materials Science, Professor Yoshihiro Furukawa and Professor Takeshi Kakegawa, Tohoku University, and Professor Toshimori Sekine, Hiroshima University for useful discussions and helpful suggestions.

The financial supports of KAKENHI (16K17782 and 26460035) is gratefully acknowledged. This research used computational resources of the HPCI system provided by Information Technology Center, The University of Tokyo and K-computer through the HPCI System Research Project (Project ID: hp160056 and hp160057). The authors also kindly acknowledge the Supercomputer Center, Institute for Solid State Physics, The University of Tokyo, for the use of its facilities.

References

1 A. Brack, Chem. Biodiversity, 2007, **4**, 665–679.
2 J. F. Kasting, Science, 1993, **259**, 920–926.
3 K. Zahnle, L. Schaefer and B. Fegley, Cold Spring Harb. Perspect. Biol., 2010, **2**, a004895.
4 S. C. Wagner, Nat. Edu. Knowledge, 2012, **3**, 15.
5 C. Higman and S. Tam, Chem. Rev., 2014, **114**, 1673–1708.
6 J. Brandes, N. Boctor, G. Cody, B. Cooper, R. Hazen and H. Yoder, Nature, 1998, **395**, 365–367.
7 A. Smirnov, D. Hausner, R. Laffers, D. R. Strongin and M. A. A. Schoonen, Geochem. Trans., 2008, **9**, 5.
8 D. P. Summers and S. Chang, Nature, 1993, **365**, 630–632.
9 G. N. Schrauzer and T. D. Guth, J. Am. Chem. Soc., 1977, **99**, 7189–7193.
10 H. Nakazawa, T. Sekine, T. Kakegawa and S. Nakazawa, Earth Planet. Sci. Lett., 2005, **235**, 356–360.
11 W. F. Bottke, D. Vokrouhlicky, D. Minton, D. Nesvorny, A. Morbidelli, R. Brasser, B. Simonson and H. F. Levison, Nature, 2012, **485**, 78–81.
12 K. Shimamura, F. Shimojo, A. Nakano and S. Tanaka, Sci. Rep., 2016, **6**, 38953.
13 Y. Furukawa, T. Samejima, H. Nakazawa and T. Kakegawa, Icarus, 2014, **231**, 77–82.
14 Y. Furukawa, T. Sekine, M. Oba, T. Kakegawa and H. Nakazawa, Nat. Geosci., 2009, **2**, 62–66.
15 Y. Furukawa, H. Nakazawa, T. Sekine, T. Kobayashi and T. Kakegawa, Earth Planet. Sci. Lett., 2015, **429**, 216–222.
16 Y. Umeda, N. Fukunaga, T. Sekine, Y. Furukawa, T. Kakegawa, T. Kobayashi and H. Nakazawa, J. Biol. Phys., 2016, **42**, 177–198.
17 C. P. Mckay, Origins Life Evol. B., 1997, **27**, 263–289.
18 G. L. Villanueva, M. J. Mumma, R. E. Novak, H. U. Käufl, P. Hartogh, T. Encrenaz, A. Tokunaga, A. Khayat and M. D. Smith, Science, 2015, **348**, 218–221.
19 E. J. Reed, L. E. Fried and J. D. Joannopoulos, Phys. Rev. Lett., 2003, **90**, 235503.
20 K. Shimamura, M. Misawa, S. Ohmura, F. Shimojo, R. K. Kalia, A. Nakano and P. Vashishta, Appl. Phys. Lett., 2016, **108**, 071901.
21 E. Skulason, T. Bligaard, S. Gudmundsdottir, F. Studt, J. Rossmeisl, F. Abild-Pedersen, T. Vegge, H. Jonsson and J. K. Norskov, Phys. Chem. Chem. Phys., 2012, **14**, 1235–1245.
22 C. J. M. van der Ham, M. T. M. Koper and D. G. H. Hetterscheid, Chem. Soc. Rev., 2014, **43**, 5183–5191.
23 J. Head and M. Zerner, Chem. Phys. Lett., 1985, **122**, 264–270.
24 P. E. Blöchl, Phys. Rev. B, 1994, **50**, 17953–17979.
25 G. Kresse and D. Joubert, Phys. Rev. B, 1999, **59**, 1758–1775.
26 J. P. Perdew, K. Burke and M. Ernzerhof, Phys. Rev. Lett., 1996, **77**, 3865–3868.
27 S. G. Louie, S. Froyen and M. L. Cohen, Phys. Rev. B, 1982, **26**, 1738–1742.
28 K.-i. Nomura, R. K. Kalia, Y. Li, A. Nakano, P. Rajak, C. Sheng,

K. Shimamura, F. Shimojo and P. Vashishta, Sci. Rep., 2016, **6**, 24109.
29 S. Grimme, J. Comp. Chem., 2006, **27**, 1787–1799.
30 J. Ihm, A. Zunger and M. L. Cohen, J. Phys. C, 1979, **12**, 4409.
31 G. Kresse and J. Hafner, Phys. Rev. B, 1994, **49**, 14251–14269.
32 F. Shimojo, R. K. Kalia, A. Nakano and P. Vashishta, Comput. Phys. Commun., 2001, **140**, 303–314.
33 E. J. Reed, L. E. Fried, W. D. Henshaw and C. M. Tarver, Phys. Rev. E, 2006, **74**, 056706.
34 R. S. Mulliken, J. Chem. Phys., 1955, **23**, 1833–1840.
35 R. S. Mulliken, J. Chem. Phys., 1955, **23**, 1841–1846.
36 S.-P. Daniel, A. Emilio and M. S. José, J. Phys. Condens. Matter, 1996, **8**, 3859–3880.
37 M. D. Segall, R. Shah, C. J. Pickard and M. C. Payne, Phys. Rev. B, 1996, **54**, 16317–16320.
38 F. Shimojo, A. Nakano, R. K. Kalia and P. Vashishta, Phys. Rev. E, 2008, **77**, 066103.
39 K. Hass, W. Schneider, A. Curioni and W. Andreoni, Science, 1998, **282**, 265–268.
40 S. Nosé, Mol. Phys., 1984, **52**, 255–268.
41 A. Curioni, M. Sprik, W. Andreoni, H. Schiffer, J. Hutter and M. Parrinello, J Am. Chem. Soc., 1997, **119**, 7218–7229.
42 F. Shimojo, R. K. Kalia, A. Nakano and P. Vashishta, Comput Phys Commun., 2001, **140**, 303 – 314.
43 D. W. Hughes and I. P. Williams, Mon. Not. R. Astron. Soc., 2000, **315**, 629–634.
44 E. Anders, Nature, 1989, **342**, 255–257.
45 B. Baldwin and Y. Sheaffer, J. Geophy. Res., 1971, **76**, 4653–4668.
46 T. Bazhenova and A. Shilov, Coord. Chem. Rev., 1995, **144**, 69–145.
47 A. Shilov, Russ. Chem. B+ , 2003, **52**, 2555–2562.
48 N. Hazari, Chem. Soc. Rev., 2010, **39**, 4044–4056.
49 N. Goldman, E. J. Reed, L. E. Fried, I. F. W. Kuo and A. Maiti, Nat. Chem., 2010, **2**, 949–954.
50 N. Goldman and I. Tamblyn, J. Phys. Chem. A, 2013, **117**, 5124–5131.
51 M. H. Vedadi and S. Haas, Appl. Phys. Lett., 2011, **99**, 154105.
52 K. Shimamura, F. Shimojo, R. Kalia, A. Nakano, K.-I. Nomura and P. Vashishta, Nano Lett., 2014, **14**, 4090–4096.
53 K. Shimamura, Y. Shibuta, S. Ohmura, R. Arifin and F. Shimojo, J. Phys.: Condens. Matter, 2016, **28**, 145001.
54 K. Shimamura, R. Arifin, T. Oguri, Y. Shibuta, S. Ohmura, F. Shimojo and S. Yamaguchi, Trans. Mat. Res. Soc. Japan, 2015, **40**, 215–218.

5 Graphics

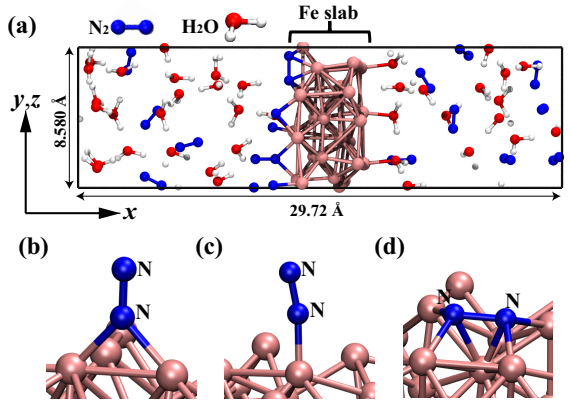

Fig. 1 (a) Initial atomic configuration of the system consisting of a Fe_{36} slab, $16N_2$, and 38 H_2O molecules. (b)-(d) Three types of adsorption of a N_2 molecule on the Fe slab.

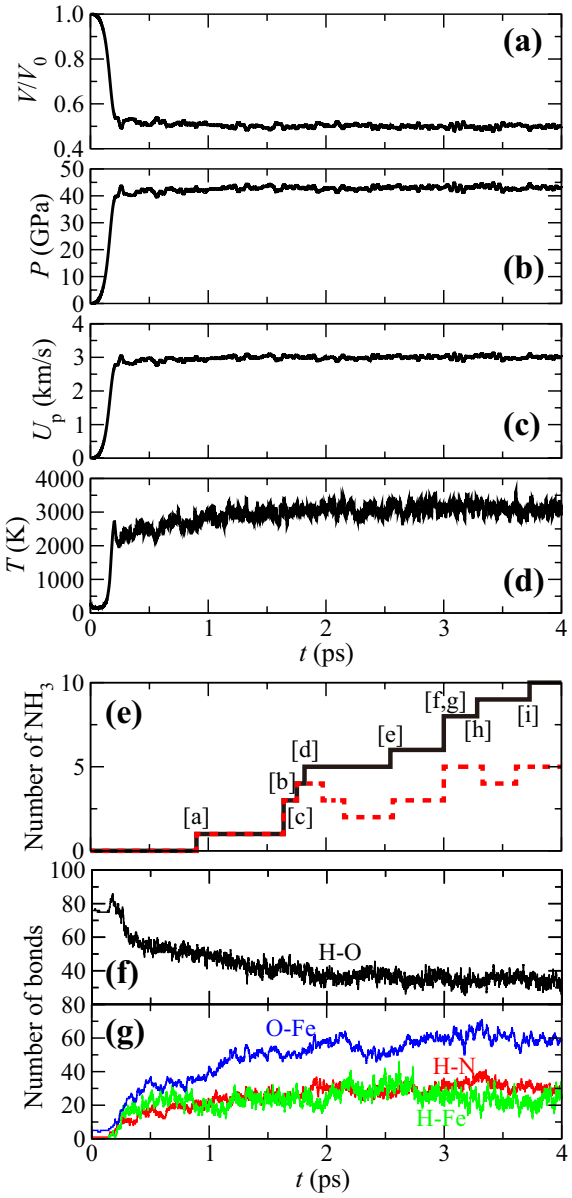

Fig. 2 Time evolution of (a) volume ratio, (b) pressure, (c) particle velocity, and (d) temperature in the 6 km/s shock-wave simulation. (e) Time evolution of cumulative number of produced NH_3 molecules or NH_4^+ (solid line) and of remaining number of produced NH_3 molecules (dashed line). (f) and (g) Time evolution of the number of H-O, H-N, H-Fe, and O-Fe bonds.

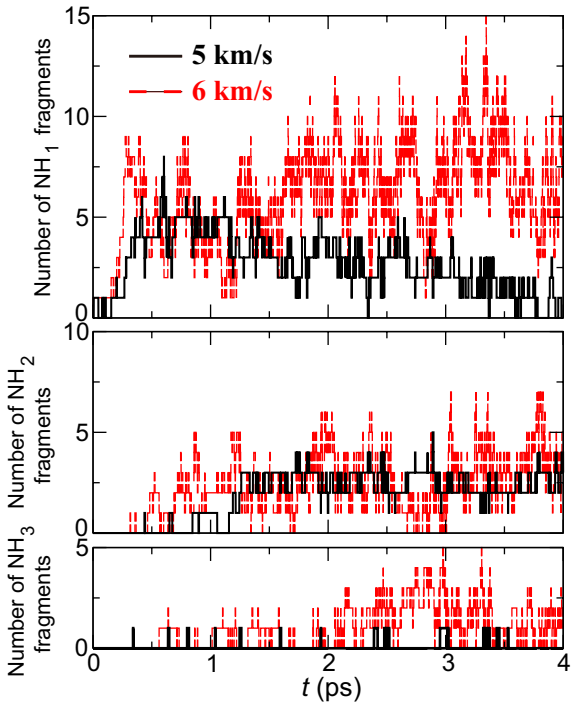

Fig. 3 Time evolution of the number of (a) NH_1 fragments, (b) NH_2 fragments, and (a) NH_3 fragments, where the black and red dashed lines represent those for the 5 and 6 km/s shock-wave simulations, respectively.

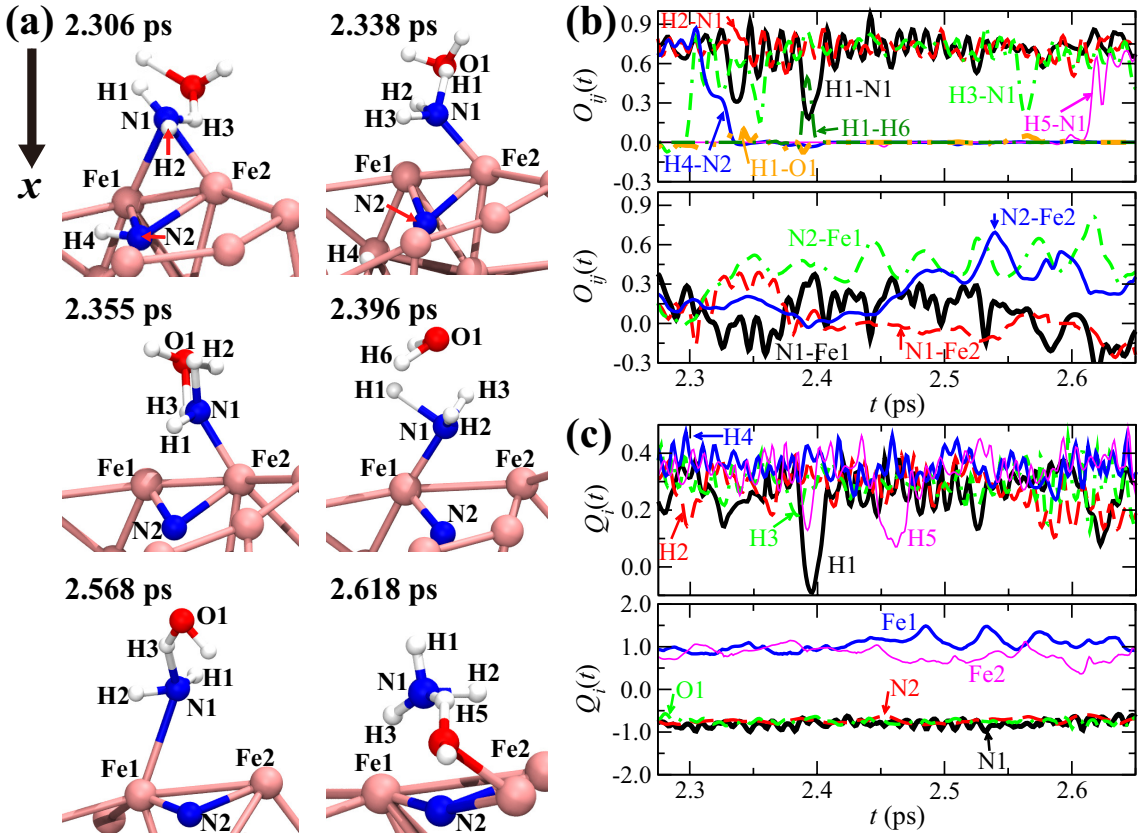

Fig. 4 (a) Atomistic configurations at 2.306, 2.338, 2.355, 2.396, 2.568, and 2.618 ps during the desorption of an NH_3 fragment from the Fe slab surface. Time evolution of (b) the bond-overlap populations $O_{ij}(t)$ and (c) the Mulliken charges $Q_i(t)$ associated with the atoms labeled in (a).

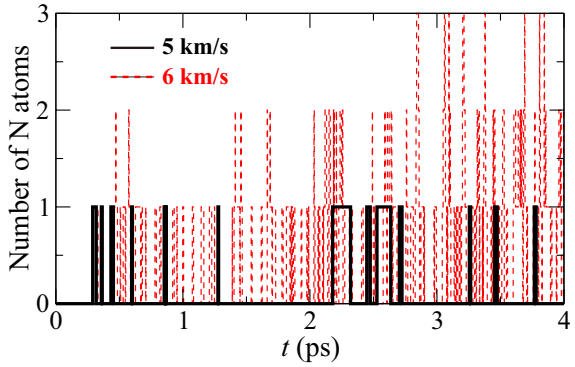

Fig. 5 Time evolution of the number of N atoms bonded to two Fe atoms (N_{2Fe}), where the black solid and red dashed lines represent those for the 5 and 6 km/s shock-wave simulations, respectively.

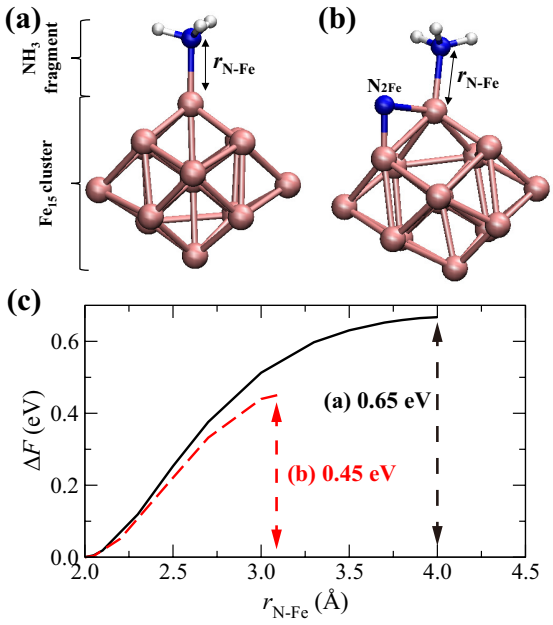

Fig. 6 Atomic configurations of the systems consisting of one Fe_{15} cluster and one NH_3 fragment (a) without and (b) with one N atom bonded to two Fe atoms (N_{2Fe}). (c) Free energy profiles at 300 K for the systems (a) and (b) as functions of the distance r_{N-Fe} between N and Fe atoms.

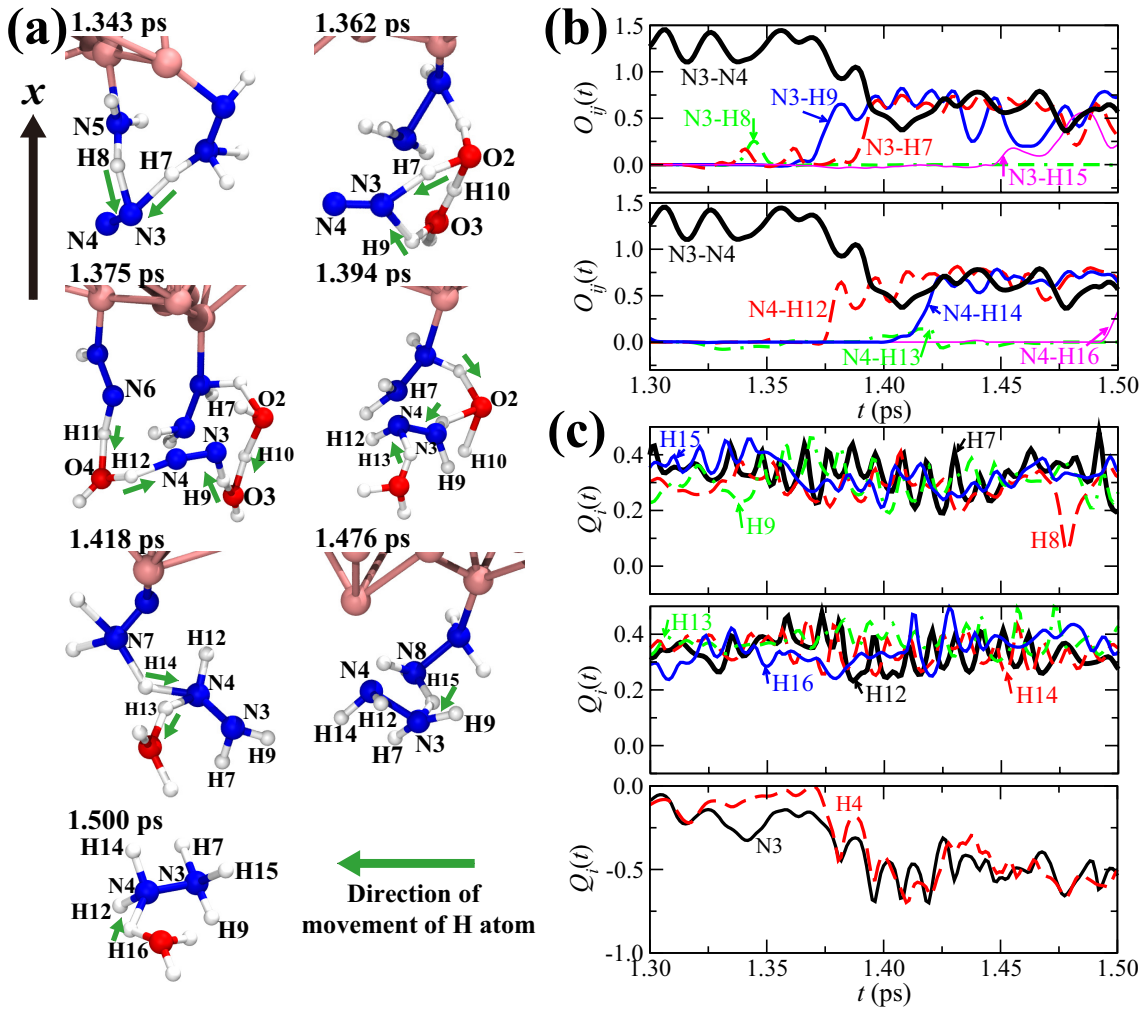

Fig. 7 (a) Atomistic configurations at 1.343, 1.362, 1.375, 1.394, 1.418, 1.476, and 1.500 ps during the formation of a $N_2H_6^{+2}$ ion from a N_2 molecule. Time evolution of (b) the bond-overlap populations $O_{ij}(t)$ and (c) the Mulliken charges $Q_i(t)$ associated with the atoms labeled in (a).

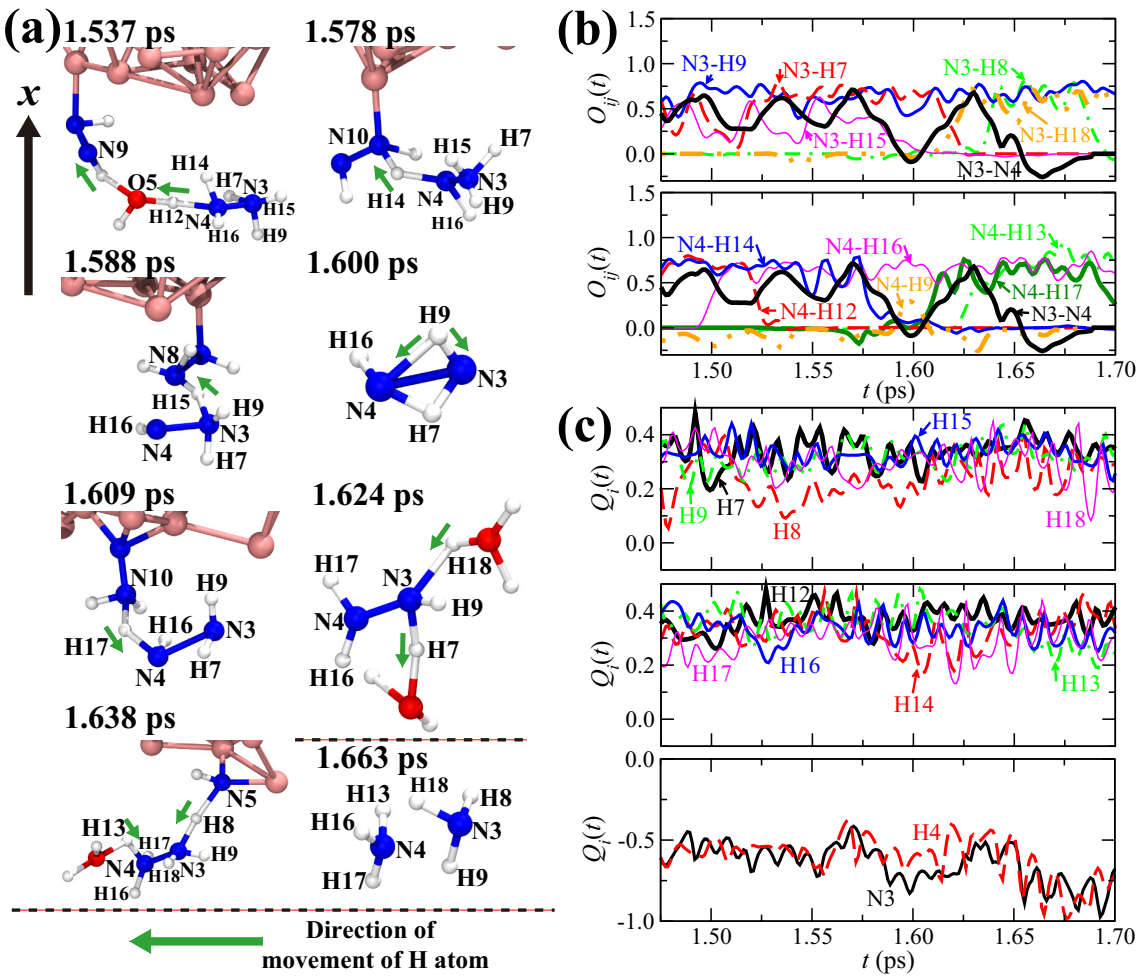

Fig. 8 (a) Atomistic configurations at 1.537, 1.578, 1.588, 1.600, 1.609, 1.624, 1.638, and 1.663 ps during the production of two NH_3 molecules by reduction of the $N_2H_6^{+2}$. Time evolution of (b) the bond-overlap populations $O_{ij}(t)$ and (c) the Mulliken charges $Q_i(t)$ associated with the atoms labeled in (a).

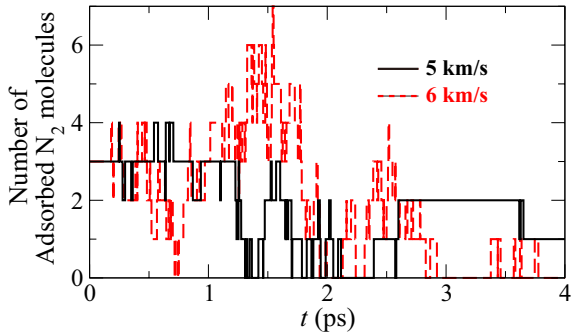

Fig. 9 Time evolution of the number of N_2 molecules bonded by more than one H atoms upright on the Fe slab surface, where the black solid and red dashed lines represent those for the 5 and 6 km/s shock-wave simulations, respectively.